nature climate change

Article

https://doi.org/10.1038/s41558-025-02245-w

Observed multi-decadal increase in the surface ocean's thermal inertia

Received: 23 July 2024

Accepted: 6 January 2025

Published online: 06 February 2025

Check for updates

Chaehyeong Lee[1,4], Hajoon Song[1,2] ✉, Yeonju Choi[1], Ajin Cho[1] & John Marshall[3]

The ocean's surface layer has a crucial role in Earth's climate, absorbing excess atmospheric heat, thereby regulating global temperatures. Here, using global daily sea surface temperature (SST) data, we document a notable increase in the persistence of SST anomalies across the global ocean since 1982. This trend is also evident in frequency space, showing a decreased variance in SSTs on timescales shorter than a month, but a slight increase on longer timescales. A simple stochastic model attributes this prolonged memory to three key factors––a deepening of the surface mixed layer, a weakening of oceanic forcing and reduced damping rates. The first two factors decrease the variance on shorter timescales, while the third increases it on longer timescales. Our findings have great relevance to the observed increase in the duration of marine heatwaves and the associated heightened thermal threats to marine organisms. Our study also suggests that the ocean's ability to sequester heat is weakening.

Sea surface temperature (SST) has an intrinsic tendency to relax back to its prior state when perturbed by atmospheric forcing[1–3]. This negative feedback mitigates positive SST anomalies through loss of energy to the atmosphere or storage within the ocean's interior. The damping rate of near-surface-ocean thermal anomalies is a very important indicator, representing the potential for the ocean to buffer climate change, particularly considering that more than 90% of Earth's excess energy due to greenhouse gas emissions has been drawn down into its interior[4–6].

The response of SST to anomalies in forcing can be represented as a simple first-order autoregressive (AR(1)) process[1] in which anomalies decay exponentially over time. This simple model aptly captures the observed red-noise power spectrum of SST. The ocean's mixed layer integrates stochastic atmospheric forcing, characterized by a white-noise spectrum, yielding a dampened SST variability at shorter timescales (less than 1 year)[1,2,7–10]. Based on this framework, the decay rate of SST anomalies depends on the heat content of the mixed layer and the efficiency of the negative feedback (damping) processes. The deepening of the mixed layer and a weakening of damping rates can extend the persistence of SST anomalies. While prolonged SST persistence leads to enhanced predictability, it also intensifies the potential threat of thermal anomalies to marine ecosystems[11–13], perhaps resulting in mortality and shifts in species composition (ref. 14 and references therein). For all these reasons, quantifying changes in SST persistence is of great importance.

The persistence of SST and its associated memory timescale have been examined using both observations and numerical models. Monthly SST anomalies in the North Pacific tend to persist for longer, associated with a deepening trend in the mixed layer[9]. The same trend has been reported for both the North Pacific and Atlantic, with Lenton et al.[15] attributing it to the weakening of negative feedback processes. Contrastingly, Ding and Li[16] suggested that both large-scale variability and local cloud–SST positive feedback is important in the North Pacific decadal changes in the monthly mean SST memory timescale.

Previous studies have primarily analysed the SST memory timescale using monthly averaged data, although the persistence of SST on timescales shorter than one month is also a crucial area of investigation. For example, the duration of marine heatwaves (MHWs), defined as events with positive SST anomalies exceeding the 90th

[1]Department of Atmospheric Sciences, Yonsei University, Seoul, Republic of Korea. [2]Division of Environmental Science & Engineering, Pohang University of Science and Technology, Pohang, Republic of Korea. [3]Department of Earth, Atmospheric and Planetary Sciences, Massachusetts Institute of Technology, Cambridge, MA, USA. [4]Present address: Department of Atmospheric and Oceanic Sciences, University of Colorado Boulder, Boulder, CO, USA. ✉e-mail: hajsong@yonsei.ac.kr

https://doi.org/10.1038/s41558-025-02245-w

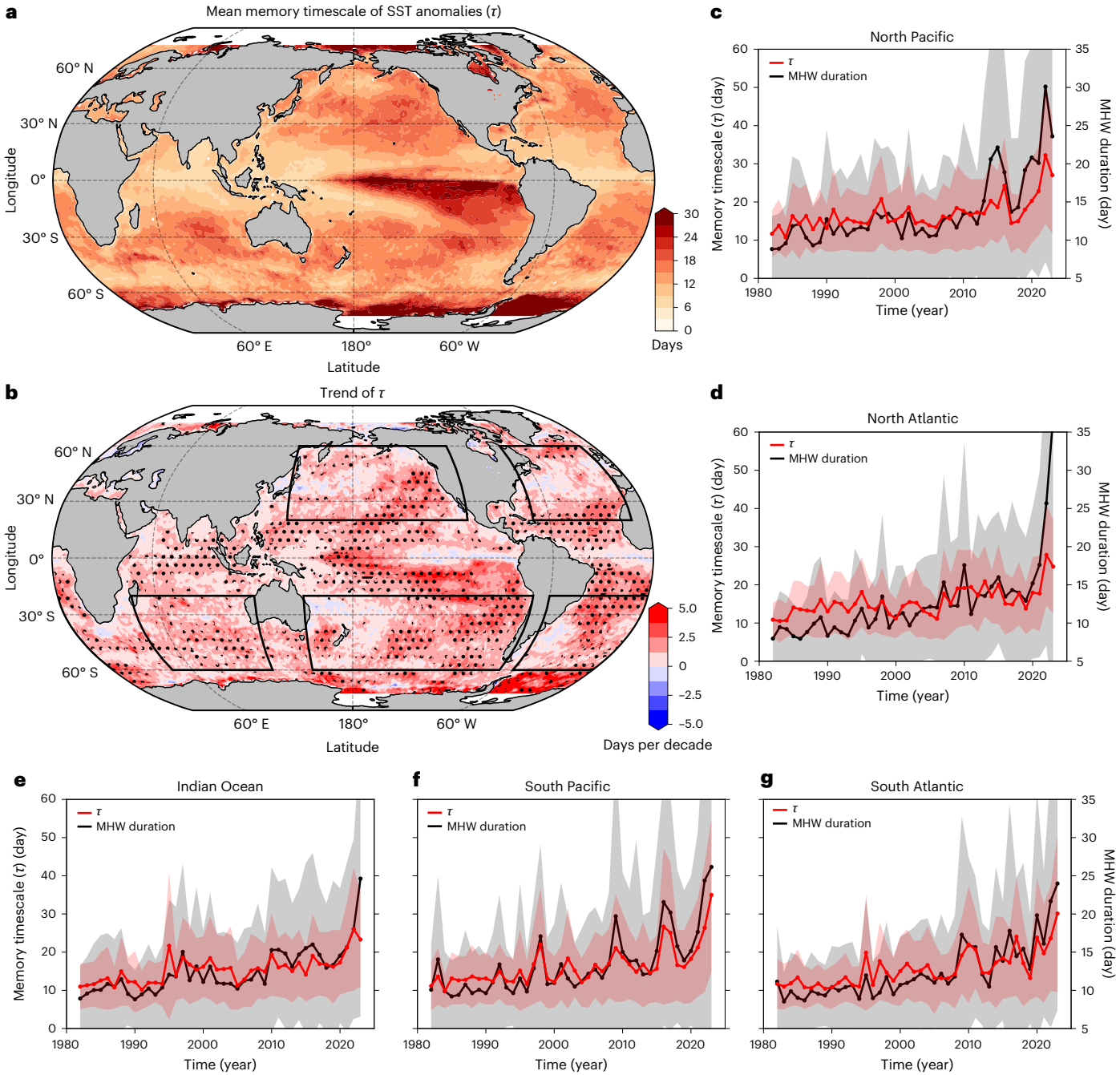

Fig. 1 | Mean memory timescales of SST anomalies and their trends. a, The mean memory timescale ($\bar{\tau}$) of SST anomalies estimated from satellite observations. **b**, The linear trend from 1982 to 2023, the black boxes indicating those regions where the time series of τ, the power spectra of the SST anomalies and the mean MLD were calculated, the dotted areas representing the regions where τ in 2023 had increased by more than 50% compared to 1982. Most of the globe shows a statistically significant increasing trend. **c**–**g**, Annual variation in the (red) memory timescale and (black) duration of MHWs from 1982 to 2023 across the five regions, with the pink and grey shading representing one standard deviation: North Pacific (**c**), North Atlantic (**d**), Indian Ocean (**e**), South Pacific (**f**) and South Atlantic (**g**).

percentile and lasting for at least five consecutive days[17,18], shows a tight correlation with the memory timescale of daily SST[19]. In eastern boundary upwelling regions, synoptic scale winds drive variations in SST on timescales of a few days, impacting nutrient distribution and primary productivity through coastal upwelling[20–23]. Additionally, marine species are sensitive to both mean temperatures and to variabilities occurring over days to weeks[24].

Despite its importance, the trend in memory timescales of daily SST has not been actively explored on the global scale. The persistence of SST is influenced by rapidly varying processes, such as surface waves and sub-mesoscale phenomena[25], and its trend may diverge from that of monthly the SST. Here the memory timescale of daily SST is evaluated using 42 years' worth of global satellite data. We found a statistically significant and notable increase in the memory timescale across major parts of the global ocean, and attempt to explain this trend using the AR(1) model.

The observed memory timescale of SST and its decadal trend

Before estimating the memory timescale of SST (τ), the daily 0.25°-resolution National Oceanic Atmospheric Administration

https://doi.org/10.1038/s41558-025-02245-w

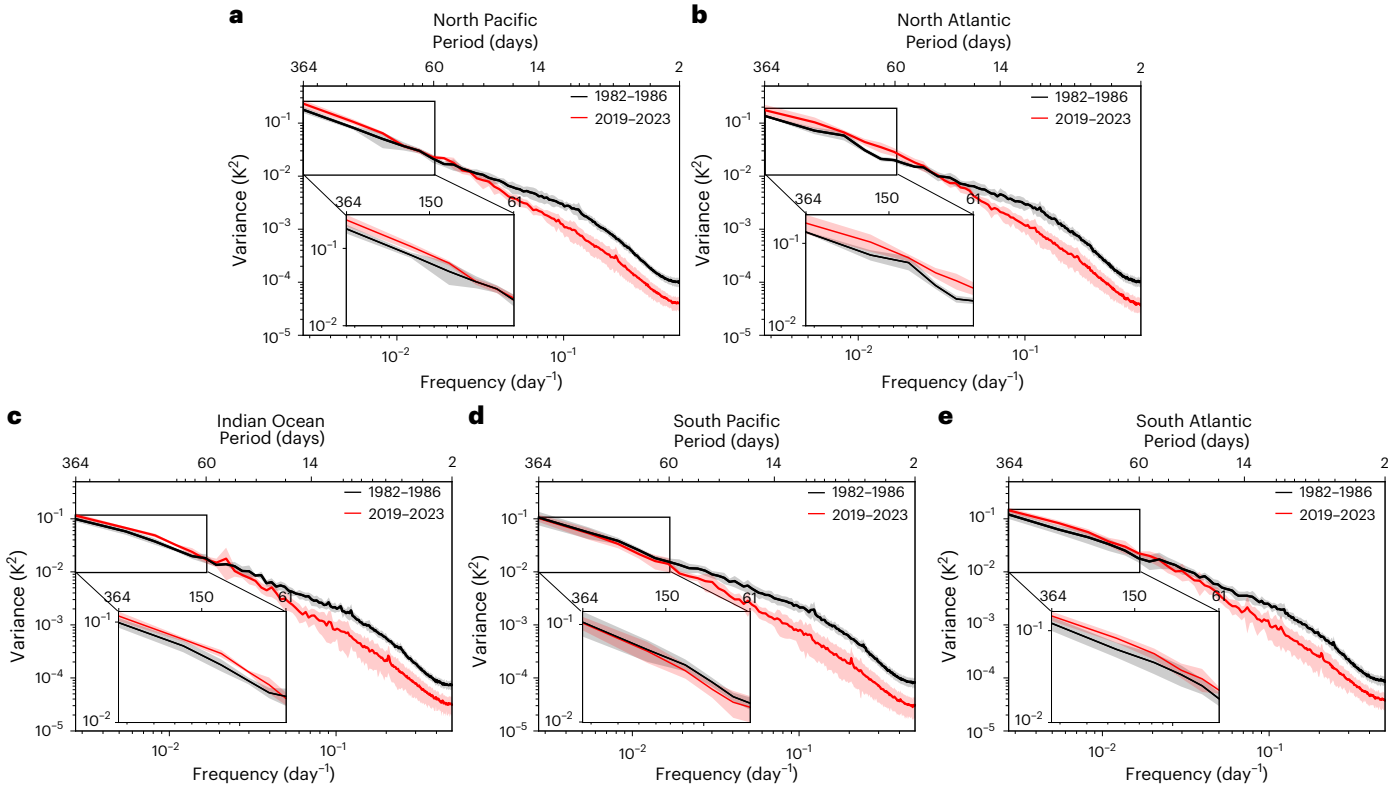

Fig. 2 | Power spectra of SST anomalies. a–e, Power spectra of SST anomalies for the five regions indicated by black boxes in Fig. 1b: North Pacific (**a**); North Atlantic (**b**); Indian Ocean (**c**); South Pacific (**d**); and South Atlantic (**e**). The averaged power spectrum for the first and last 5 years of the analysed period are shown by black and red lines, respectively, the pink and grey shading represents one standard deviation. Insets zoom in on periods greater than 60 days.

Optimum Interpolation SST dataset[26] was interpolated onto a 1°-resolution grid and fitted to the AR(1) model using a 10 day lag autocorrelation for each year to find the damping coefficient (λ in equation (1), Methods). Our approach was equivalent to finding the time at which the autocorrelation coefficient fell below $1/e$, as in ref. 19. Broadly, we found that the memory timescales of daily SST are shorter than 20 days, except in the eastern equatorial Pacific where they exceed 30 days (Fig. 1a). Other regions with long memory timescales include the eastern North Pacific, the regions north of the Gulf Stream and Kuroshio Current, the Agulhas Retroflection and the eastern southern Indian Ocean. By contrast, the equatorial western Pacific, Indian, Atlantic and much of the Southern Oceans have memory timescales shorter than 10 days.

Strikingly, the memory timescale of daily SST exhibits a statistically significant increasing trend over the global ocean almost everywhere (Fig. 1b). The basin-averaged memory timescale has nearly doubled over the last 42 years (Fig. 1c–g). For example, in the eastern North Pacific, the SST memory timescale has been increasing at a rate of 2.5 days per decade—a full 50% increase over the last 42 years. Even at lower latitudes, between 20° S and 20° N, the average trend is roughly 2 days per decade, implying a doubling of the memory timescale over the last 42 years. The extension of the memory timescale of daily SST is also evident from the autocorrelation analysis of SST anomalies alone (Methods and Extended Data Figs. 1 and 2), emphasizing the robustness of this signal.

This rising trend in the global ocean is potentially linked to the observed increase in the duration of MHWs, which has extended by more than 30 days in roughly 80% of the global ocean from 1982 to 2023[27] (Fig. 1c–g). These findings underscore a notable and concerning shift in the ocean's behaviour, allowing extreme SST anomalies to persist for much longer periods over the last four decades, potentially posing a greater threat to marine ecosystems.

Power spectra analysis has corroborated the extension of the memory timescales of daily SST across the major ocean basins. Comparing the first 5 years (black lines in Fig. 2) with the last 5 years (red lines in Fig. 2), we can see two notable changes over the last four decades. Variance at higher frequencies was reduced during the 2019–2023 period compared to 1982–1986—a statistically significant signature across all major ocean basins. By contrast, there was a slight increase in power at lower frequencies in the last 5 years (insets in Fig. 2). The diminished variance at high frequencies implies reduced SST fluctuation on timescales shorter than a month, indicating extended memory timescales of daily SST, consistent with changes in the autocorrelation coefficient.

Mechanisms behind the prolongation of SST memory

The global trend of increasing SST memory timescale was investigated using a simple thermodynamic balance rooted in the AR(1) model, which accounts for both atmospheric and oceanic processes (Methods). An increase in SST memory timescale can occur through four primary mechanisms—an increase in the heat content of the mixed layer, a decrease in damping rates, and changes in atmospheric and/or oceanic forcing. The deepening of the mixed layer, and hence the increase in heat content, reduces the variance of SST anomalies at high frequencies. Conversely, a decreasing trend in damping results in increased variance at low frequencies. The atmospheric forcing term is often perceived to be white noise[8], whereas the oceanic forcing term shows decreasing variance towards higher frequency on timescales shorter than a few months[10]. We quantified the contribution of these four mechanisms in the AR(1) model by allowing changes in each variable of interest while keeping the others fixed at climatological values.

Recent findings have revealed, counter-intuitively, an increase in mixed-layer depth (MLD) occurring concurrently with a strengthening in

https://doi.org/10.1038/s41558-025-02245-w

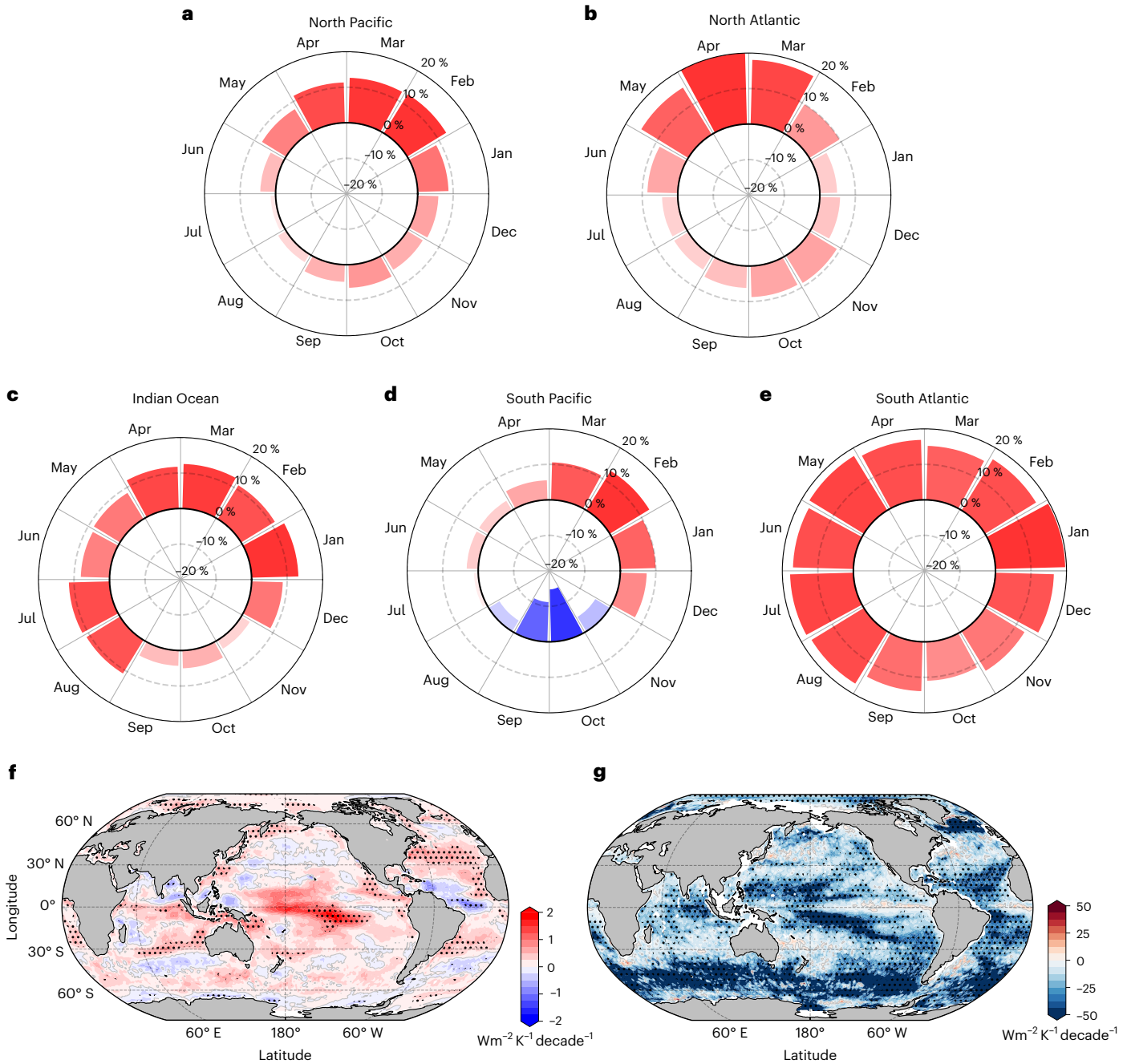

Fig. 3 | Changes in MLD and damping coefficients. a–e, The mean percentage differences in monthly MLD between the last (2019–2023) and first (1982–1986) 5 years for the five regions marked by black boxes in Fig. 1b: North Pacific (**a**), North Atlantic (**b**), Indian Ocean (c), South Pacific (**d**) and South Atlantic (**e**). The MLD was derived from 1970 to 2018[28]. **f**,**g**, The linear trend in the atmospheric damping coefficient (λ_a) and the oceanic damping coefficient (λ_o) from 1982 to 2023, respectively, with dotted regions having statistically significant trends at a 95% confidence level.

upper-ocean stratification[28]. Except for the austral fall in the South Pacific, the mixed layer has deepened roughly 10% over the last 40 years, with the North Atlantic exhibiting a nearly 20% deepening in April (Fig. 3a–e). This is equivalent to on the order of a 10% increase in the mixed-layer heat content, slowing down the decay of SST anomalies. The solution of the AR(1) model suggests that this change reduces the power at high frequencies (red lines in Fig. 4), consistent with shifts in the SST power spectra across all major ocean basins (Fig. 2). However, this change alone cannot explain the observed decrease in SST variance (black lines in Fig. 4).

Another contributing factor to the increased SST memory timescale is the damping coefficient, which, based on the AR(1) model, modifies power mainly at low frequencies. The damping coefficient can be decomposed into two distinct components, one associated with the atmosphere, the other with the ocean. The atmospheric damping coefficient can be derived through differentiation of the bulk formulae with respect to the SST[29], revealing contributions from long-wave radiation and latent and sensible heat fluxes (Methods). Using fifth-generation European Centre for Medium-Range Weather Forecasts atmospheric reanalysis of the global climate (ERA5) data, we found an atmospheric damping coefficient of roughly 30 W m^{-2} K^{-1} in the middle latitudes (Extended Data Fig. 3a), with the latent heat flux being the largest contributor (Extended Data Fig. 3c–e). This is consistent with previous studies that employed lagged covariance methods between surface heat-flux anomalies and SST anomalies[10,30,31].

https://doi.org/10.1038/s41558-025-02245-w

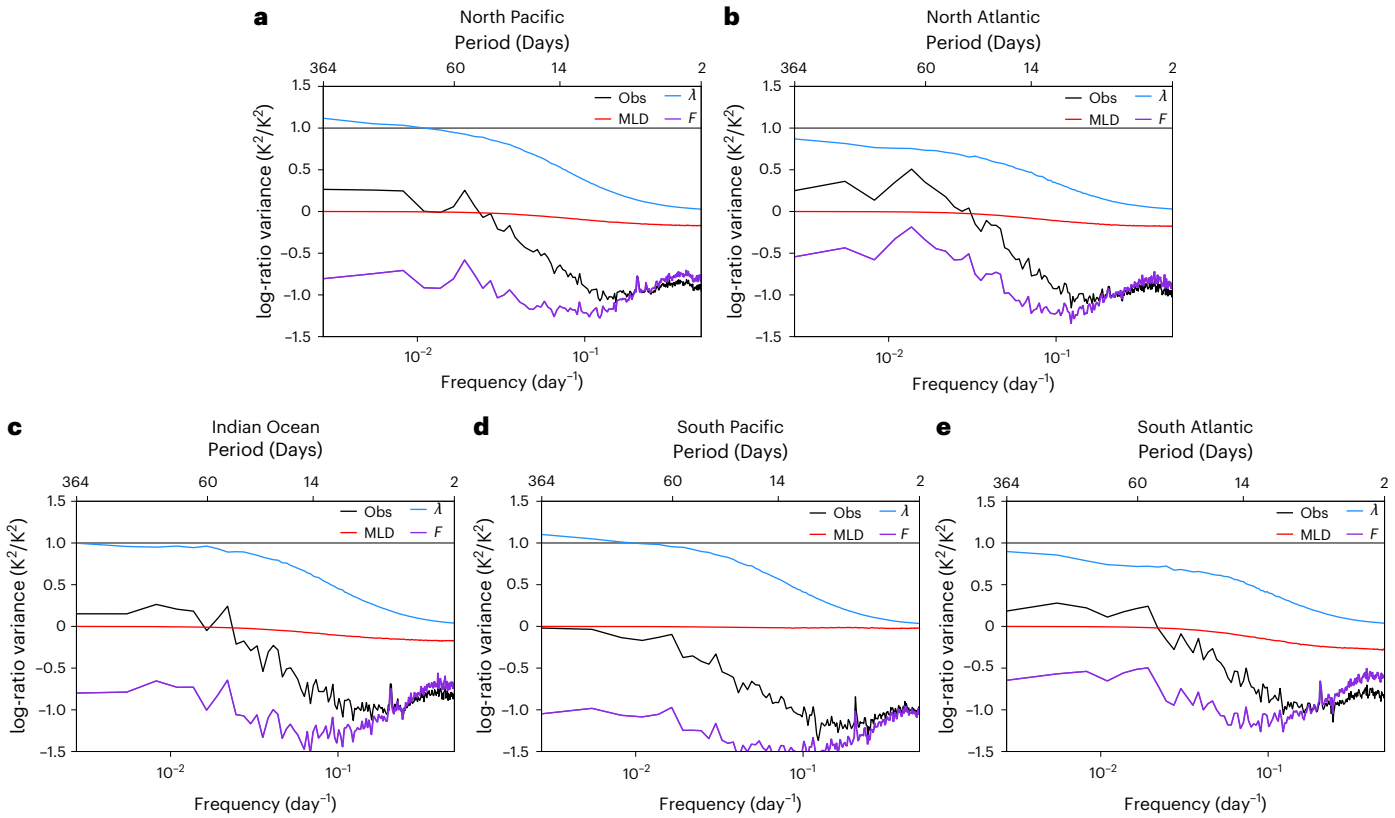

Fig. 4 | Factors contributing to changes in SST anomaly variances. a–e, The log-ratio of the observed (obs) (black curves) and calculated (coloured curves) power spectra of SST anomalies between the first and last 5 years. The log-ratio of the power spectra of SST anomalies due to the damping coefficient ($\lambda = \lambda_a + \lambda_o$), the MLD ($H$) and the forcing ($F = F_a + F_o$) are represented in blue, red and purple, respectively. Calculation of the power spectra of the SST anomalies was based on the analytic solution of our AR(1) stochastic model (equation (16)).

The atmospheric damping coefficient has had a positive trend in many global ocean regions over the last 42 years (Fig. 3f). This is most prominent in the tropical Pacific, Indian Ocean and extratropical Atlantic. This would lead to a shortening of the SST memory timescale due to damping to the atmosphere, in contrast to the observed prolongation of SST memory. While a few regions do show a negative atmospheric damping trend, this is relatively modest, having a value of roughly 0.5 W m^{-2} decade^{-1}, equivalent to an increase of 2 W m^{-2} in heat loss for a 1 °C increase in SST over the last 42 years. Therefore, it is unlikely that surface heat fluxes can account for increased SST memory.

The oceanic damping coefficient is generally larger than those of the atmosphere in specific regions[10]. It encapsulates several processes, such as lateral mixing, vertical entrainment and advection by ocean currents[10,31]. While it can be estimated using lagged covariance, analogously to the atmospheric damping coefficient[10], here we computed it as a residual by subtracting the atmospheric damping coefficient from the total damping coefficient estimated from satellite SST and climatological MLD (Methods). The resulting oceanic damping coefficients exceed those of the atmosphere, and elevated values were revealed in the Southern Ocean and the northern North Atlantic (Extended Data Fig. 3b), as shown in a previous study[10].

The trend in ocean damping is predominantly negative across almost all global oceans (Fig. 3g). This reduction aligns with the strengthened upper-ocean stratification, as measured by the buoyancy frequency at the pycnocline and as observed across the global ocean[28]. Increased upper-ocean stratification makes heat sequestration into the ocean interior less effective, allowing SST anomalies to grow, and increasing SST variance at low frequencies, as suggested by the AR(1) model. Although our analysis was limited to timescales shorter than 365 days and did not fully resolve the white-noise signal region, the power spectra consistently show a trend towards increased variance at lower frequencies (insets in Fig. 2). This suggests that the decreased damping coefficient in recent years has contributed to the prolongation of SST memory timescales by amplifying the slowly varying component of SST. Comparing the first and last 5 years, the damping coefficient's contribution to the changes in the SST power spectra is most notable at low frequencies, potentially increasing SST variance by an order of magnitude (blue curves in Fig. 4), though this effect is offset by changes in the forcing.

The forcing term, comprising both atmospheric and oceanic contributions, was estimated indirectly using the solution of the AR(1) model (Methods). Over the last 42 years, the contribution of forcing to the variance in SST anomalies has decreased across all frequency ranges in all ocean basins (purple curves in Fig. 4). This negative contribution offsets the positive impact of the decreasing damping coefficient, resulting in a slight increase in SST variance at low frequencies. At high frequencies, changes in the forcing term have significantly contributed to the change in SST variance, leading to a slower decay of SST anomalies in recent years.

The forcing term accounts for the combined effects of the atmosphere and ocean, with the atmospheric contribution again estimated using ERA5 data. Oceanic forcing is then obtained as the residual (equation (16)). On timescales shorter than approximately 10 days, atmospheric forcing shows a decreasing variance with frequency, inconsistent with the white-noise assumption in the AR(1) model (Extended Data Fig. 4). However, this inconsistency is expected to have had a limited effect on extending SST memory timescale because the atmospheric forcing remained relatively unchanged during the study period (Extended Data Fig. 4). Thus, we conclude that changes in oceanic forcing over the last four decades are probably responsible

for the decreased SST variance at high frequencies, resulting in a longer SST memory timescale.

Discussion

The ocean plays a crucial role in Earth's energy balance, storing over 90% of the excess heat in Earth's system[4–6]. Using daily SST observations, we have shown that the global ocean has become less effective at damping SST anomalies over the last four decades. The SST power spectra have revealed decreased variance at high frequencies (less than a month) and increased variance at low frequencies, together indicating a slower decay rate of SST anomalies. The former is due to reduced oceanic forcing and an MLD deepening trend, whereas the latter is due to a weakening in oceanic damping associated with the observed strengthening of upper-ocean stratification[28]. These upper-ocean changes suggest a trend towards increased heat storage in the upper ocean and reduced sequestration into its interior, and an increasing likelihood of prolonged heatwaves and hence a threat to near-surface marine ecosystems.

Future projections for the upper ocean have included stronger stratification and a shallower mixed layer[32,33], with implications for SST memory timescales. Shi et al.[34] argued that shoaling of the MLD under the Shared Socioeconomic Pathway 5-8.5 scenario may decrease the persistence of the annual SST. This contrasts with the projected increase in the persistence of the daily SST reported in Li and Thompson[35], computed using large ensembles of Earth system models, and attributed to a reduced damping coefficient and changes in forcing. These opposing projections of persistence of the annual and daily SST imply complex interactions between multiple dynamic and thermodynamic processes that underlie the damping of SST anomalies.

Using a simple stochastic model, we have determined how the surface ocean has evolved into a state that can sustain temperature anomalies for longer periods. This memory timescale cannot be identified by conventional statistical measures, such as mean and variance, because even datasets with the same mean and variance can have different memory timescales. Given the importance of memory timescales in understanding the thermal state of the ocean and its impact on marine ecosystems, a thorough investigation of trends in SST memory timescales and their underlying drivers—across daily, monthly and annual scales—is essential for accurate projections of the ocean's heat storage in a warming climate.

Online content

Any methods, additional references, Nature Portfolio reporting summaries, source data, extended data, supplementary information, acknowledgements, peer review information; details of author contributions and competing interests; and statements of data and code availability are available at https://doi.org/10.1038/s41558-025-02245-w.

References

1. Frankignoul, C. & Hasselmann, K. Stochastic climate models, Part II Application to sea-surface temperature anomalies and thermocline variability. *Tellus A: Dyn. Meteorol. Oceanogr.* **29**, 289–305 (1977).
2. Deser, C., Alexander, M. A., Xie, S.-P. & Phillips, A. S. Sea surface temperature variability: Patterns and mechanisms. *Annu. Rev. Mar. Sci.* **2**, 115–143 (2010).
3. Xie, S.-P. A dynamic ocean–atmosphere model of the tropical Atlantic decadal variability. *J. Clim.* **12**, 64–70 (1999).
4. Rhein, M. & Rintoul, S. R. et al. in *Climate Change 2013: The Physical Science Basis* (eds Stocker, T. F. et al.) Ch. 3 (Cambridge Univ. Press, 2013).
5. Trenberth, K. E., Fasullo, J. T. & Balmaseda, M. A. Earth's energy imbalance. *J. Clim.* **27**, 3129–3144 (2014).
6. von Schuckmann, K. et al. Heat stored in the earth system 1960–2020: where does the energy go? *Earth Syst. Sci. Data* **15**, 1675–1709 (2023).
7. Hasselmann, K. Stochastic climate models Part I. Theory. *Tellus* **28**, 473–485 (1976).
8. Marshall, J. & Plumb, R. A. in *Atmosphere, Ocean and Climate Dynamics: An Introductory Text* (eds Dmowska, R., Hartmann, D. & Rossby, T.) 262–266 (Elsevier, 2008).
9. Boulton, C. A. & Lenton, T. M. Slowing down of North Pacific climate variability and its implications for abrupt ecosystem change. *Proc. Natl Acad. Sci. USA* **112**, 11496–11501 (2015).
10. Patrizio, C. R. & Thompson, D. W. J. Understanding the role of ocean dynamics in midlatitude sea surface temperature variability using a simple stochastic climate model. *J. Clim.* **35**, 3313–3333 (2022).
11. Frölicher, T. L. & Laufkötter, C. Emerging risks from marine heat waves. *Nat. Commun.* **9**, 650 (2018).
12. Mills, K. E. et al. Fisheries management in a changing climate: lessons from the 2012 ocean heat wave in the Northwest Atlantic. *Oceanography* **26**, 191–195 (2013).
13. Moore, J. A. Y. et al. Unprecedented mass bleaching and loss of coral across 12° of latitude in Western Australia in 2010–11. *PLoS ONE* **7**, 51807 (2012).
14. Smale, D. A. et al. Marine heatwaves threaten global biodiversity and the provision of ecosystem services. *Nat. Clim. Change* **9**, 306–312 (2019).
15. Lenton, T. M., Dakos, V., Bathiany, S. & Scheffer, M. Observed trends in the magnitude and persistence of monthly temperature variability. *Sci. Rep.* **7**, 5940 (2017).
16. Ding, R. & Li, J. Decadal and seasonal dependence of North Pacific sea surface temperature persistence. *J. Geophys. Res.: Atmos.* **114**, D01105 (2009).
17. Hobday, A. J. et al. A hierarchical approach to defining marine heatwaves. *Prog. Oceanogr.* **141**, 227–238 (2016).
18. Hobday, A. J. et al. Categorizing and naming marine heatwaves. *Oceanography* **31**, 162–173 (2018).
19. Oliver, E. C. J. et al. Marine heatwaves. *Annu. Rev. Mar. Sci.* **13**, 313–342 (2021).
20. Botsford, L. W., Lawrence, C. A., Dever, E. P., Hastings, A. & Largier, J. Effects of variable winds on biological productivity on continental shelves in coastal upwelling systems. *Deep-Sea Res. II: Top. Stud. Oceanogr.* **53**, 3116–3140 (2006).
21. García-Reyes, M., Largier, J. L. & Sydeman, W. J. Synoptic-scale upwelling indices and predictions of phyto- and zooplankton populations. *Prog. Oceanogr.* **120**, 177–188 (2014).
22. Aguirre, C., Garreaud, R. D. & Rutllant, J. A. Surface ocean response to synoptic-scale variability in wind stress and heat fluxes off south-central Chile. *Dyn. Atmos. Oceans* **65**, 64–85 (2014).
23. Aguirre, C., Rojas, M., Garreaud, R. D. & Rahn, D. A. Role of synoptic activity on projected changes in upwelling-favourable winds at the ocean's eastern boundaries. *npj Clim. Atmos. Sci.* **2**, 44 (2019).
24. Dillon, M. E. et al. Life in the frequency domain: the biological impacts of changes in climate variability at multiple time scales. *Integr. Comp. Biol.* **56**, 14–30 (2016).
25. Bulgin, C. E., Merchant, C. J. & Ferreira, D. Tendencies, variability and persistence of sea surface temperature anomalies. *Sci. Rep.* **10**, 7986 (2020).
26. Reynolds, R. W. et al. Daily high-resolution-blended analyses for sea surface temperature. *J. Clim.* **20**, 5473–5496 (2007).
27. Oliver, E. C. J. et al. Longer and more frequent marine heatwaves over the past century. *Nat. Commun.* **9**, 1324 (2018).
28. Sallée, J. B. et al. Summertime increases in upper-ocean stratification and mixed-layer depth. *Nature* **591**, 592–598 (2021).
29. Klinger, B. A. & Haine, T. W. N. *Ocean Circulation in Three Dimensions* Ch. 4 (Cambridge Univ. Press, 2019).

30. Frankignoul, C. & Kestenare, E. The surface heat flux feedback. Part I: Estimates from observations in the Atlantic and the North Pacific. *Clim. Dyn.* **19**, 633–648 (2002).
31. Hausmann, U., Czaja, A. & Marshall, J. Estimates of air–sea feedbacks on sea surface temperature anomalies in the Southern Ocean. *J. Clim.* **29**, 439–454 (2016).
32. Kwiatkowski, L. et al. Twenty-first century ocean warming, acidification, deoxygenation, and upper-ocean nutrient and primary production decline from CMIP6 model projections. *Biogeosciences* **17**, 3439–3470 (2020).
33. Jo, A. R. et al. Future amplification of sea surface temperature seasonality due to enhanced ocean stratification. *Geophys. Res. Lett.* **49**, 2022–098607 (2022).
34. Shi, H. et al. Global decline in ocean memory over the 21st century. *Sci. Adv.* **8**, 3468 (2022).
35. Li, J. & Thompson, D. W. J. Widespread changes in surface temperature persistence under climate change. *Nature* **599**, 425–430 (2021).

Methods

Data sources and statistical processing

Our study utilized five variables—the air–sea total heat flux, SST, 2 m air temperature (that is, measured at 2 m above the surface), 10 m wind and MLD. The SST data were obtained from the Daily Optimum Interpolation Sea Surface Temperature (DOISST) versions 2.0 and 2.1 dataset[26,36,37], provided by the National Centers for Environmental Information. The SST anomalies were computed by removing both the seasonal cycle and the 42-year linear trend from the daily data.

Although slowly varying climate variabilities, such as the El Niño–Southern Oscillation and the Interdecadal Pacific Oscillation, were present in the SST anomalies, their removal had a minimal impact on the analysis and did not alter the main conclusions.

To explore the consistency and quality of the DOISST data, we compared its SST power spectrum with that from in situ temperature observations from the North Atlantic over a four-decade period. The comparison revealed strong agreement between the two datasets, suggesting that the DOISST dataset faithfully captures variance across all frequency ranges in both historical and recent periods (Supplementary Fig. 1). We assumed that the satellite data from the earlier periods may not have been as reliable as those from more recent years, and so the trends in τ over the last 32 years (1992–2023) were also calculated. The results closely resembled those from the last 42 years (Fig. 1b), showing statistically significant trends over large areas across the global ocean (Supplementary Fig. 2).

The 2m atmospheric temperature and 10m wind data were from the European Centre for Medium-Range Weather Forecasts Reanalysis V5 (ERA5) dataset[38]. The monthly mean MLD and its linear trend were obtained from Sallée et al.[28], who compiled over three million profiles from ship-based conductivity, temperature and depth data, Argo floats, and sensors attached to marine mammals, providing a 0.5°-resolution MLD determined based on a density criterion. These variables were projected onto a 1° regular grid for analysis.

The study spanned 42 years, from 1982 to 2023, encompassing a period of overlap between the DOISST and ERA5 datasets. Although DOISST provided SST data from September 1981, we excluded this year due to its incomplete coverage of the full calendar year. For the same reason, 2024 was not considered in the analysis.

The trend of the SST memory timescale was estimated using the Theil–Sen estimator[39,40] (95% interval of the sampled slope)—an unbiased metric that has little sensitivity to outliers. The Mann–Kendall rank test (95% interval of the confidence level) was then employed to determine the significance of the trend[41–44].

Estimation of surface thermal memory timescale

AR(1) model. Non-seasonal SST variabilities are often examined using a simplified model in which the SST anomalies respond to stochastic atmospheric forcing and are then linearly damped (for example, refs. 1,7,8). Assuming a uniform MLD, this model can be written

$$C_0\frac{\mathrm{d}T'}{\mathrm{d}t} = F - \lambda T', \tag{1}$$

where $C_0 = \rho c_p H$ is the heat content of the mixed layer, ρ is the density of seawater, c_p is its specific heat and H is the MLD. In equation (1), F and λ represent the stochastic forcing and damping of SST anomalies, respectively. The terms on the right-hand side encompass not only atmospheric but also oceanic dynamic processes, such as temperature advection by both wind-driven gyres and Ekman currents[10].

The solution to (1) is given by

$$T'(t) = T'(t-\delta t)\exp\left(-\frac{\lambda}{C_0}\delta t\right) + \int_{t-\delta t}^{t}\exp\left(\frac{\lambda}{C_0}(t'-t)\right)\frac{F(t')}{C_0}\mathrm{d}t'. \tag{2}$$

where the first and second terms on the right-hand side represent the exponential decay of the SST anomaly and the accumulated effects of stochastic forcing on the SST anomaly over the interval $t-\delta t$ and t, respectively. The anomaly decay rate can be characterized by a memory timescale ($\tau = C_0/\lambda$). This is essentially identical to the AR(1) model

$$T'_n = \phi T'_{n-1} + \epsilon_n, \tag{3}$$

where the subscripts denote the time step, ϕ is the lag-1 autocorrelation coefficient and ϵ_n is the white-noise forcing[45,46]. Thus, if F is a white-noise process, the memory timescale, τ, can be obtained from the lag-1 autocorrelation coefficient, ϕ, by relating the first terms of equations (3) and (2) and using a daily time interval, thus:

$$\tau = \frac{C_0}{\lambda} = -\frac{1}{\ln\phi}. \tag{4}$$

When F is not entirely white-noise forcing, the estimation of τ can be biased. Indeed Patrizio and Thompson[10] suggested that the oceanic forcing term has weak persistence, which could lead to an underestimation of the damping coefficient, λ. However, the influence of red-noise forcing diminishes over time, and the degree of bias is suppressed as the lag used to estimate λ increases.

The AR(1) model allows T'_n to be expressed using T'_{n-k}—the temperature at lag k—because it can be written successively as

$$\begin{aligned} T'_n &= \phi T'_{n-1} + \epsilon_n \\ &= \phi\left(\phi T'_{n-2} + \epsilon_{n-1}\right) + \epsilon_n \\ &\vdots \\ &= \phi^k T'_{n-k} + \sum_{i=0}^{k-1}\phi^i\epsilon_{n-i}. \end{aligned} \tag{5}$$

Estimating ϕ requires only one data point because it is always 1 at lag-0. Based on a simple toy model experiment similar to that described in Patrizio and Thompson[10], we chose the 10-day lag autocorrelation coefficient, $\phi_{10} = \phi^{10}$, to estimate $\tau = -10/\ln\phi_{10}$. This choice significantly reduced the bias to less than 5% (Supplementary Fig. 3), which is negligible compared to the computed trend in λ using satellite SST data.

Arctangent regressive model. While the AR(1) model effectively captures the processes controlling SST anomalies, the e-folding timescale is determined solely by the lag-10 autocorrelation coefficient. An alternative approach involves the direct estimation of the surface thermal memory timescale from the autocorrelation of daily SST anomalies for each year. Given the discrete nature of the autocorrelation coefficient of daily SST anomalies, we first fit the autocorrelation using the following empirical arctangent function:

$$\phi_k = 1 - \frac{\tan^{-1}(\alpha k)}{2}. \tag{6}$$

where ϕ_k is the autocorrelation coefficient, k is the lag value and α is the parameter that needs to be determined to minimize the root-mean-squared error of this arctangent function with respect to the autocorrelation. The memory timescale, τ, is found by identifying the point at which the autocorrelation coefficient falls to $1/e$—that is, $\frac{1}{e} = 1 - \frac{\tan^{-1}(\alpha\tau)}{2}$—which can be rearranged and written thus

$$\tau = \frac{\tan(2-2/e)}{\alpha}. \tag{7}$$

In the estimation of τ, the number of lag values (k) can be varied to best fit the autocorrelation using equation (6). The 42-year mean τ and its trend, estimated by fitting equation (6) to the lag-10

autocorrelation, are similar to those obtained from the AR(1) model (Fig. 1a,b and Extended Data Figs. 1c and 2c). Similarly to the AR(1) model, a higher value of k tends to decrease the 42-year mean τ, notably in the eastern North Pacific, North Atlantic and western South Pacific, although the spatial patterns remain comparable with the memory timescale of the SST anomalies estimated using the AR(1) model (Extended Data Fig. 1b–e). Moreover, the memory timescale trends estimated using equation (6) also show a consistent tendency to extend the memory timescale globally, regardless of k (Extended Data Fig. 2b–e). These results suggest that the extended SST memory timescale is a robust signal.

Estimation of atmospheric and oceanic damping coefficient

The damping coefficient, λ, in equation (1), can be partitioned into two components—the rate of damping through surface heat flux (λ_a) and through oceanic processes (λ_o). λ_a can be further decomposed into three contributions—λ_{rad}, λ_{sh} and λ_{lh}—associated with long-wave radiation (Q_B), sensible heat flux (Q_H) and latent heat flux (Q_L), respectively[29],

$$\begin{aligned}\lambda_a &= \lambda_{rad} + \lambda_{sh} + \lambda_{lh} \\ &= \left(\frac{\partial Q_B}{\partial T} + \frac{\partial Q_H}{\partial T} + \frac{\partial Q_L}{\partial T}\right)\Big|_{T=T_A},\end{aligned} \tag{8}$$

where T_A is the 2m atmospheric temperature obtained from ERA5.

The terms in equation (8) are estimated by linearizing the bulk formulas[47,48], as follows[49–51]:

$$\frac{\partial Q_B}{\partial T} = 4\sigma T^3, \tag{9}$$

$$\frac{\partial Q_H}{\partial T} = \rho_a c_p C_H U, \tag{10}$$

$$\frac{\partial Q_L}{\partial T} = -\Lambda_v C_E U \frac{q_1 q_2}{T^2} \exp\left(\frac{q_2}{T}\right). \tag{11}$$

The names, units and values of the variables and parameters in equations (9)–(11) were adapted from ref. 48 and are provided in Supplementary Table 1.

λ_a was estimated daily, and its trend was computed from 1982 to 2023, similarly to τ. Then, λ_o—the damping coefficient representing oceanic processes—was simply computed as the residual of λ and λ_a

$$\lambda_o = \lambda - \lambda_a. \tag{12}$$

Estimation of atmospheric forcing

The atmospheric forcing term, F_a, can be derived from the anomalies of total heat exchange between the ocean and atmosphere (Q'_{net}) (ref. 10) decomposed Q'_{net} into two terms—atmospheric forcing, F_a, which is independent of SST, and the damping rate, which is proportional to the atmospheric damping coefficient, λ_a, and the SST anomaly, T', as follows:

$$F_a = Q'_{net} + \lambda_a T'. \tag{13}$$

where Q_{net} is obtained by summing up the short- and long-wave radiative heat flux and sensible and latent heat flux obtained from ERA5. Again, the seasonality and long-term trend were removed for computing Q'_{net}.

Spectral analysis of SST anomalies

The spectra of SST anomalies are useful for diagnosing changes in the observed SST memory timescale. As shown in Marshall and Plumb[8], the solution for the SST anomalies in equation (1) can be written

$$T' = \mathrm{Re}(\hat{T}'_\omega \exp(i\omega t)), \tag{14}$$

where $\hat{T}'_\omega$ is the amplitude of the SST anomalies at frequency ω, and Re(·) denotes the real part. Substituting equation (14) into equation (1), and taking the product with its conjugate, yields the amplitude of SST anomalies as

$$\left(\hat{T}'_\omega\right)^2 = \left(\frac{\hat{F}_\omega}{C_0}\right)^2 \frac{1}{\omega^2 + \omega_c^2}, \tag{15}$$

where $\hat{F}_\omega$ is the amplitude of the stochastic heat exchange between the atmosphere and the ocean at ω, and $\omega_c = \lambda/C_0 = (\tau)^{-1}$.

Patrizio and Thompson[10] examined SST anomalies using a stochastic model considering both atmospheric and oceanic forcing, such that $F = F_a + F_o$, where F_a and F_o represent the atmospheric and oceanic forcing, respectively. By setting $F'_a = \mathrm{Re}(\hat{F}_{\omega,a} \exp(i\omega t))$ and $F'_o = \mathrm{Re}(\hat{F}_{\omega,o} \exp(i\omega t))$ as the SST anomalies[8], the solution for $\hat{T}'_\omega$ becomes

$$\left(\hat{T}'_\omega\right)^2 = \left(\frac{\hat{F}_{\omega,a} + \hat{F}_{\omega,o}}{C_0}\right)^2 \frac{1}{\omega^2 + \omega_c^2}, \tag{16}$$

where $\hat{F}_{\omega,a}$ and $\hat{F}_{\omega,o}$ are the amplitude of forcing at frequency ω associated with the atmosphere and ocean, respectively.

The power spectra of SST anomalies show two distinct characteristics, exhibiting both red- and white-noise features, depending on the amplitude of ω relative to ω_c. At high frequencies ($\omega \gg \omega_c$), the amplitude, $\hat{T}'_\omega$, can be approximated by $\hat{F}_\omega/(C_0\omega)$. Under the assumption of constant $\hat{F}_\omega$, this limit suggests a decline in SST anomaly variability with frequency, yielding a red-noise power spectrum. In this regime, changes in C_0 can shift the power spectra of SST anomalies upwards or downwards with no significant changes in $\hat{F}_\omega$. Specifically, an increase in C_0 can lower the $\hat{T}'_\omega$, indicating that the deepening of the mixed layer and the subsequent increase in its heat content can reduce the variability of SST anomalies at a frequency greater than ω_c, aligning with observational findings (Figs. 2 and 3a–e).

At low frequencies ($\omega \ll \omega_c$), the amplitude $\hat{T}'_\omega$ can be approximated by $\hat{F}_\omega/\lambda$ (or $\tau\hat{F}_\omega/C_0$), leading to a frequency-independent white-noise response, again under the assumption of constant $\hat{F}_\omega$. In this limit, the negative feedback represented by the damping rate, λ, plays a critical role in the decay of SST anomalies. A decrease in λ implies a slower removal of heat from the mixed layer, which elevates $\hat{T}'_\omega$ at low frequency and makes slowly varying SST anomalies more prominent in the time series (Fig. 2). Thus, the reduced damping rate contributes to the longer persistence of SST anomalies. Additionally, it can shift the critical frequency, ω_c, to lower frequencies, expanding the red-noise region.

The stochastic forcing, F, is often perceived to have white-noise characteristics, allowing for the assumption of constant $\hat{F}_\omega$. On timescales longer than a few months, this assumption is reasonable for both atmospheric and oceanic forcing, but the oceanic forcing shows decreasing power on timescales shorter than a few months[10]. Here, we estimated $\hat{F}_\omega$ for the first and last 5 years by fitting equation (15) to the observed $\hat{T}'_\omega$ using the climatological damping coefficient and MLD, its difference shown by the purple curve in Fig. 4.

Then $\hat{F}_\omega$ is partitioned into $\hat{F}_{\omega,a}$ and $\hat{F}_{\omega,o}$. $\hat{F}_{\omega,a}$ is directly computed using the ERA5 dataset, and $\hat{F}_{\omega,o}$ is estimated as a residual. Interestingly, the amplitude of the atmospheric forcing also shows declining power at timescales shorter than 2 weeks when evaluated using ERA5 data (Extended Data Fig. 4). An evaluation of $\hat{F}_{\omega,a}$ over decadal intervals from 1982 to 2023 revealed no significant changes across all ocean basins (Extended Data Fig. 4), suggesting that the shift in the SST anomaly power spectrum was not driven by the changes in $\hat{F}_{\omega,a}$.

Data availability

Details regarding the source database utilized in this study can be found at the following URLs: https://doi.org/10.5067/GHAAO-4BC21 (ref. 52) and https://doi.org/10.24381/cds.bd0915c6 (ref. 38). The global maps illustrating the trend and climatology MLD fields discussed in this paper are available via Zenodo at https://doi.org/10.5281/zenodo.4073174 (ref. 53).

Code availability

The analytical code employed for the results and Supplementary Information in this paper can be accessed at https://github.com/ChaehyeongLee/ThermalMemory.git (ref. 54).

References

36. Banzon, V., Smith, T. M., Chin, T. M., Liu, C. & Hankins, W. A long-term record of blended satellite and in situ sea-surface temperature for climate monitoring, modeling and environmental studies. *Earth Syst. Sci. Data* **8**, 165–176 (2016).
37. Huang, B. et al. Improvements of the Daily Optimum Interpolation Sea Surface Temperature (DOISST) version 2.1. *J. Clim.* **34**, 2923–2939 (2021).
38. Hersbach, H. et al. The ERA5 global reanalysis. *Q. J. R. Meteorol. Soci.* **146**, 1999–2049 (2020).
39. Sen, P. K. Estimates of the regression coefficient based on Kendall's tau. *J. Am. Stat. Assoc.* **63**, 1379–1389 (1968).
40. Theil, H. in *Henri Theil's Contributions to Economics and Econometrics* Vol. 23 (eds Raj, B. & Koerts, J.) 345–381 (Springer, 1992).
41. Mann, H. B. Nonparametric tests against trend. *Econometrica* **13**, 245–259 (1945).
42. Kendall, M. G. *Rank Correlation Methods* (Griffin, 1948).
43. Gilbert, R. O. *Statistical Methods for Environmental Pollution Monitoring* (Wiley, 1987).
44. Hussain, M. & Mahmud, I. pyMannKendall: a Python package for non parametric Mann Kendall family of trend tests. *J. Open Source Softw.* **4**, 1556 (2019).
45. Box, G. E. P., Jenkins, G. M. & Reinsel, G. C. *Autocorrelation Function and Spectrum of Stationary Processes in Time Series Analysis : Forecasting and Control* 3rd edn, 46–59 (Prentice Hall, 1994).
46. Bhattacharya, P. K. & Burman, P. *Theory and Methods of Statistics* 1st edn, 431–489 (Academic Press, 2016).
47. Roll, H. U. *Physics of the Marine Atmosphere* (Academic, 1965).
48. Large, W. G. & Yeager, S. G. *Diurnal to Decadal Global Forcing for Ocean and Sea-Ice Models: The Data Sets and Flux Climatologies*. NCAR/TN–460+STR, NCAR Technical Note (Univ. Corporation for Atmospheric Research, 2004).
49. Hausmann, U., Czaja, A. & Marshall, J. Mechanisms controlling the SST air–sea heat flux feedback and its dependence on spatial scale. *Clim. Dyn.* **48**, 1297–1307 (2017).
50. Yang, P., Jing, Z. & Wu, L. An assessment of representation of oceanic mesoscale eddy–atmosphere interaction in the current generation of general circulation models and reanalyses. *Geophys. Res. Lett.* **45**, 11856–11865 (2018).
51. Yuan, M., Li, F., Ma, X. & Yang, P. Spatio-temporal variability of surface turbulent heat flux feedback for mesoscale sea surface temperature anomaly in the global ocean. *Front. Mar. Sci.* **9**, 957796 (2022).
52. NASA/JPL GHRSST Level 4 AVHRR_OI Global blended sea surface temperature analysis (GDS2) from NCEI. *NASA Physical Oceanography Distributed Active Archive Center* https://doi.org/10.5067/GHAAO-4BC21 (2020).
53. Sallée, J.-B. et al. Fifty-year changes of the world ocean's surface layer in response to climate change. *Zenodo* https://doi.org/10.5281/zenodo.5776180 (2021).
54. Lee, C. ChaehyeongLee/ThermalMemory: V1.0.0. *Zenodo* https://doi.org/10.5281/zenodo.13863062 (2024).

Acknowledgements

H.S. was supported by a National Research Foundation of Korea grant funded by the Korean government (2018R1A5A1024958 and 2022R1A2C1009792). J.M. was supported by the Physical Oceanography program of the National Aeronautics and Space Administration (6945064) and the Massachusetts Institute of Technology–Goddard Institute for Space Studies cooperative agreement.

Author contributions

H.S. designed the study. C.L. and H.S. performed the analysis. C.L. created the figures. Y.C., A.C. and J.M. helped in the investigation. C.L. wrote the original draft and C.L., H.S., Y.C. and J.M. reviewed and edited the paper.

Competing interests

The authors declare no competing interests.

Additional information

Extended data is available for this paper at https://doi.org/10.1038/s41558-025-02245-w.

Supplementary information The online version contains supplementary material available at https://doi.org/10.1038/s41558-025-02245-w.

Correspondence and requests for materials should be addressed to Hajoon Song.

Peer review information *Nature Climate Change* thanks the anonymous reviewers for their contribution to the peer review of this work.

https://doi.org/10.1038/s41558-025-02245-w

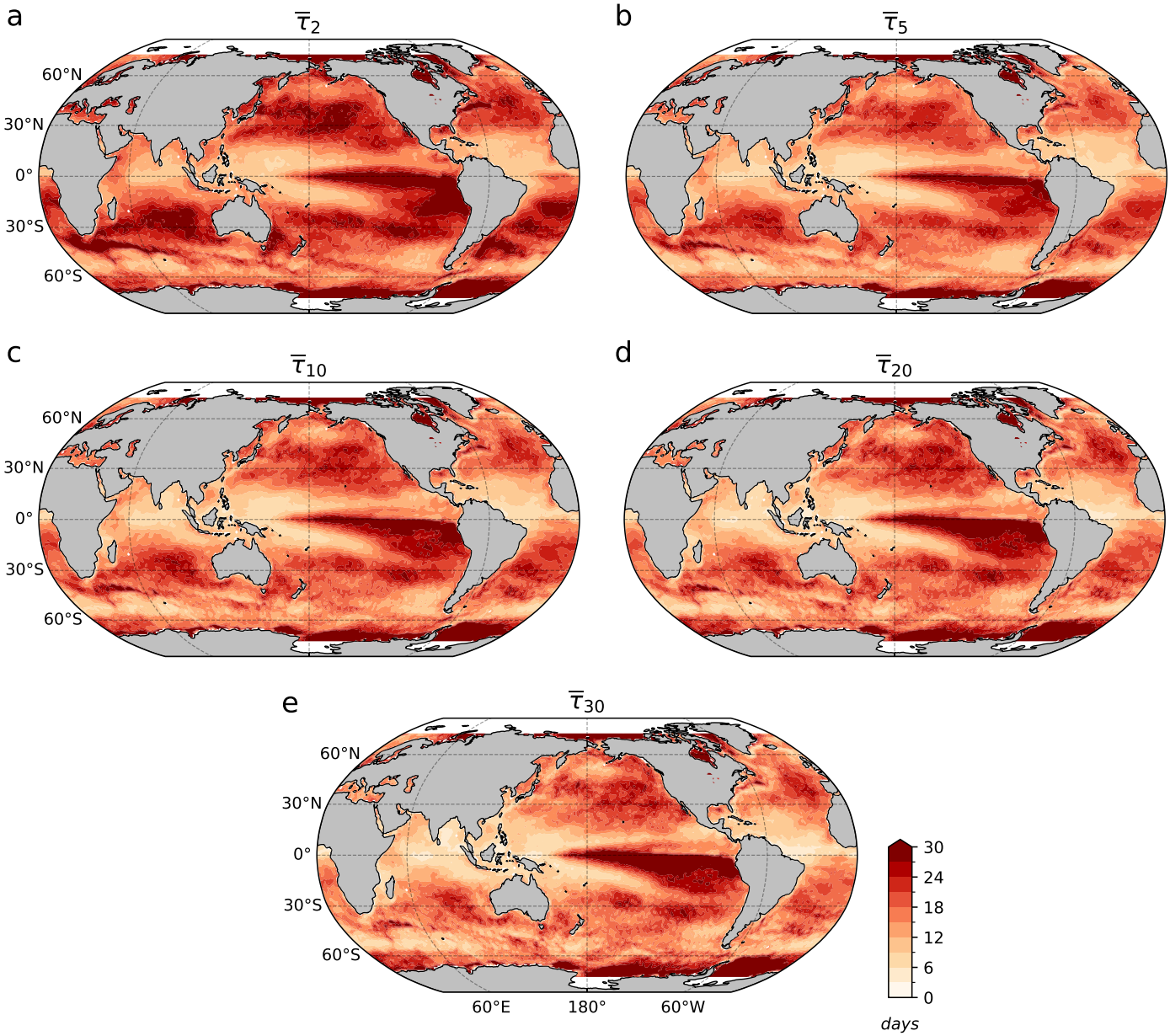

Extended Data Fig. 1 | The mean memory timescales obtained by fitting an arctangent function. a-e. The mean memory timescales ($\overline{\tau}$) of SST anomalies over a 42-year period (1982-2023). Optimal coefficients for the arctangent function are determined using 2, 5, 10, 20, and 30 consecutive autocorrelation coefficients of SST anomalies, spanning from 0-lag to the lag ($n-1$).

https://doi.org/10.1038/s41558-025-02245-w

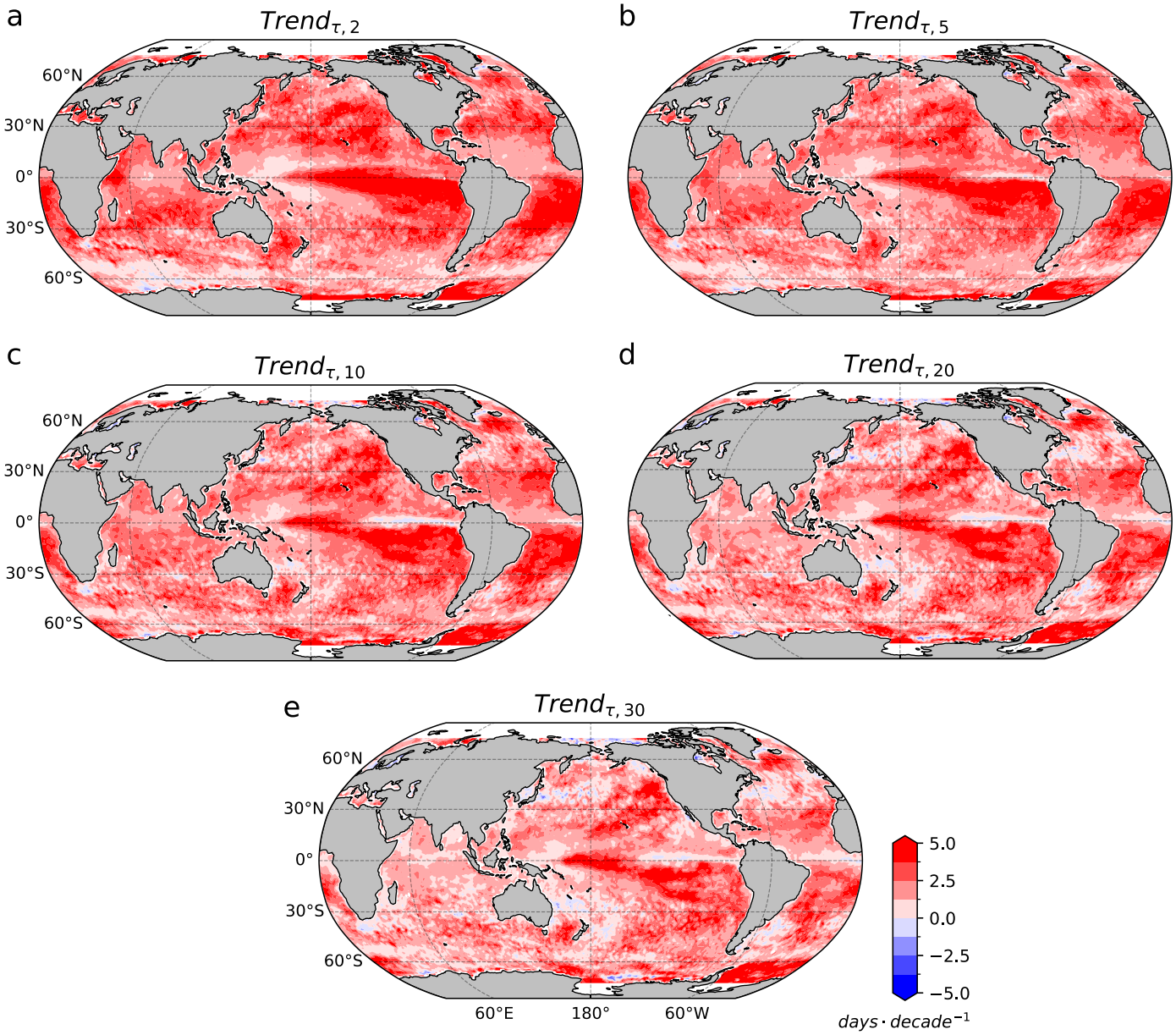

Extended Data Fig. 2 | The trend in the mean memory timescales obtained by fitting an arctangent function. a-e. The linear trend of the memory timescale is calculated using the same arctangent model used to produce the means shown in Extended Data Fig. 1a–e. from 1982 to 2023, respectively.

https://doi.org/10.1038/s41558-025-02245-w

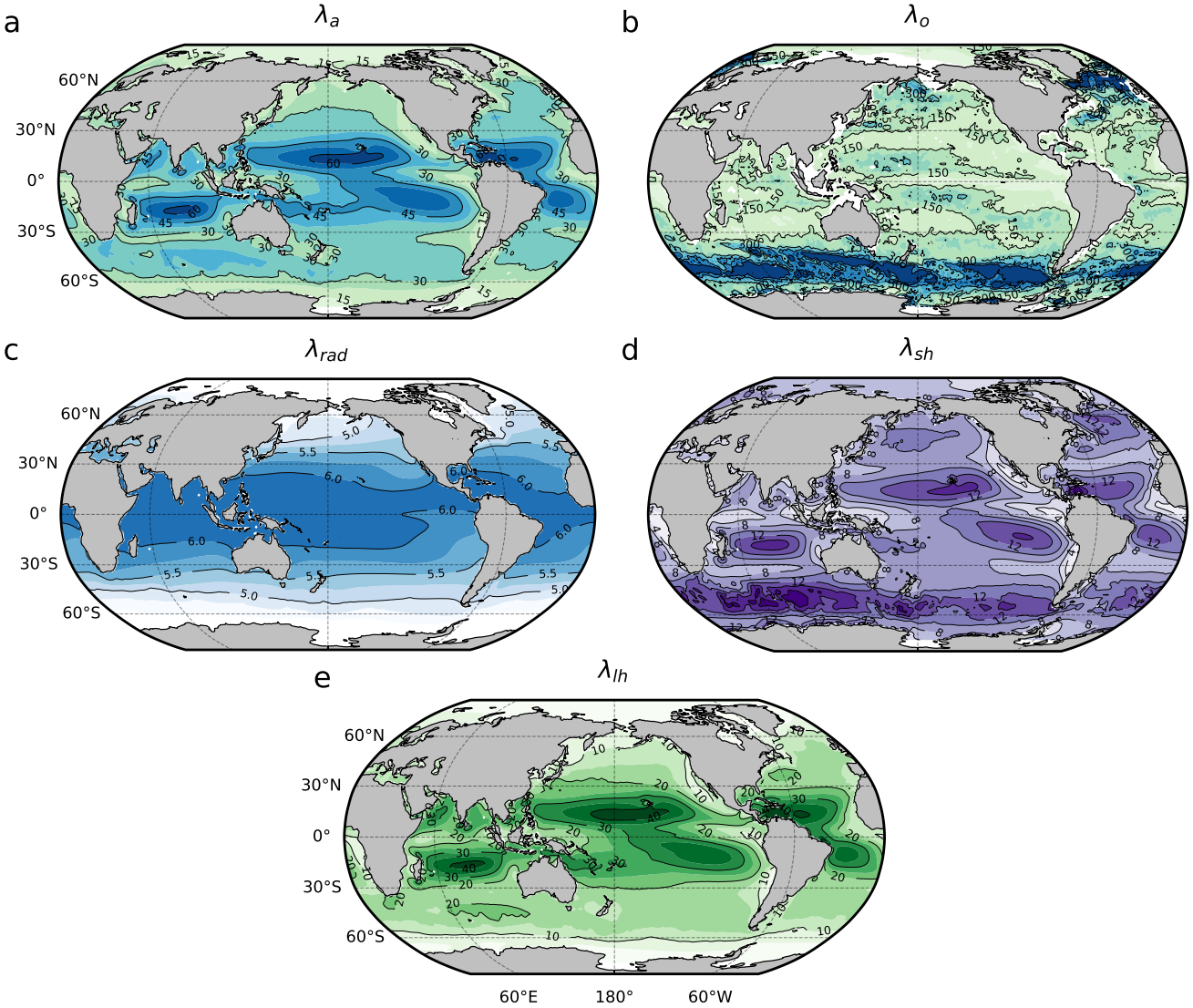

Extended Data Fig. 3 | Mean damping coefficients. a-b. Mean atmospheric (λ_a) and mean oceanic (λ_o) damping coefficient over the last 42 years. The atmospheric damping coefficient is decomposed into three contributions: **c.** long-wave radiation (λ_{rad}), **d.** sensible heat flux (λ_{sh}), and **e.** latent heat flux (λ_{lh}). The units are in W m^{-2} K^{-1}.

https://doi.org/10.1038/s41558-025-02245-w

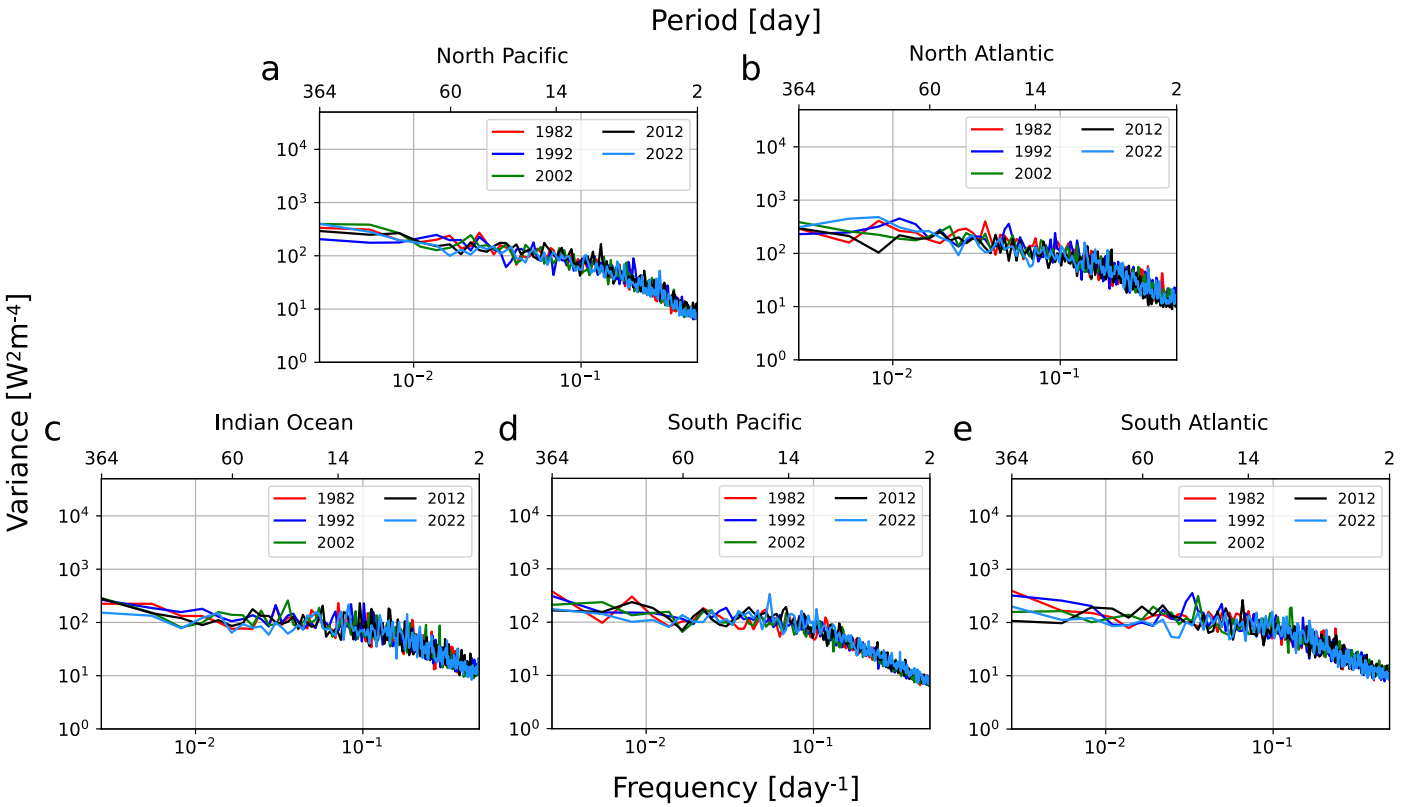

Extended Data Fig. 4 | Power spectra of atmospheric forcing. a-e. Power spectra of annual atmospheric forcing ($\hat{F}^2_{\omega,a}$) for the five regions, denoted by black boxes in Fig. 1b, are presented in every 10-year interval from 1982 to 2023.